

FUSE Observations of Galactic and Intrinsic Absorption in the Spectrum of the Seyfert 1 Galaxy 2MASX J21362313-6224008¹

Massimiliano Bonamente

*Physics Department, The University of Alabama in Huntsville, John Wright Dr., OB201,
Huntsville, AL 35899*

bonamem@email.uah.edu

and

W. Van Dyke Dixon

*Department of Physics and Astronomy, The Johns Hopkins University, 3400 North Charles
Street, Baltimore, MD 21218*

wvd@pha.jhu.edu

ABSTRACT

We present the far-ultraviolet spectrum of the Seyfert 1 galaxy 2MASX J21362313-6224008 obtained with the *Far Ultraviolet Spectroscopic Explorer (FUSE)*. The spectrum features absorption from Galactic O VI at two velocities and redshifted H I Lyman β and γ , C II, C III, and O VI. The redshifted absorption features represent a single kinematic component blueshifted by $\sim 310 \text{ km s}^{-1}$ relative to the AGN. We use photoionization models to derive constraints on the physical parameters of the absorbing gas. An alternative interpretation for the absorption lines is also proposed, whereby the absorbing gas is associated with an intervening galaxy cluster.

Subject headings: galaxies: individual (2MASX J21362313-6224008)—galaxies: ISM — ultraviolet: galaxies — galaxies: clusters: general

¹Based on observations made with the NASA-CNES-CSA *Far Ultraviolet Spectroscopic Explorer*. *FUSE* is operated for NASA by the Johns Hopkins University under NASA contract NAS5-32985.

1. INTRODUCTION

A large fraction of Seyfert 1 galaxies exhibits intrinsic UV absorption associated with the active galactic nucleus (AGN). The absorption lines are commonly blueshifted with respect to the source, indicating that the absorbing material undergoes a net radial outflow (e.g., Crenshaw et al. 1999). The absorbing material is interpreted as photoionized gas with ionization parameter $U \sim 0.01 - 0.1$ and total hydrogen column density $N_H \sim 10^{18} - 10^{21} \text{ cm}^{-2}$ (Kriss et al. 2000, 2003; Romano et al. 2002).

In this paper we present the results of a 37 ks observation of 2MASX J21362313-6224008, a Seyfert 1 galaxy with a measured redshift $z = 0.0588$ (Hewitt & Burbidge 1991) and visual magnitude $V=15.2$ mag (Remillard et al. 1986), with the *Far Ultraviolet Spectroscopic Explorer* (*FUSE*). The available X-ray HEAO-1 data of the source (also identified as 1H2129-624 and H2132-626) were analyzed by Remillard et al. (1986), who derive a luminosity $L_{2-10 \text{ keV}} = 3 \times 10^{44} \text{ erg s}^{-1}$, which is on the bright end of the quasar luminosity function (George et al. 2000). The object was observed in soft X-rays by *ROSAT*; the *ROSAT* All-Sky Bright Source Catalogue (Voges et al. 1999) and the *ROSAT* Bright Survey (Schwope et al. 2000) detect a strong X-ray source at the location of our target, which is identified as 1RXS J213623.1-622400. (Its quoted X-ray flux may be contaminated by up to 10% by the faint source 1RXS J213530.1-623005 approximately 12 arcmin to the southwest.) *EUVE* observed the source during its All-Sky Survey, but the short exposure time resulted only in an upper limit (Marshall et al. 1995). The spectral energy distribution (SED) of 2MASX J21362313-6224008 is shown in Fig. 1.

2. OBSERVATIONS AND DATA REDUCTION

FUSE consists of four separate optical systems. Two employ LiF coatings and are sensitive to wavelengths from 990 to 1187 Å, while the other two use SiC coatings, which provide reflectivity to wavelengths as short as 905 Å. The four channels overlap between 990 and 1070 Å. For a complete description of the instrument, see Moos et al. (2000) and Sahnou et al. (2000).

The *FUSE* spectrum of 2MASX J21362313-6224008 (data set D9030401) was obtained in 10 separate exposures on 2003 May 25-26. The total integration time was 37 ks, of which 12 ks were obtained during orbital night. All observations were made through the $30'' \times 30''$ (LWRS) aperture. The data were reduced using version 2.4 of the CalFUSE

²The *CalFUSE Pipeline Reference Guide* is available at http://fuse.pha.jhu.edu/analysis/pipeline_reference.html.

calibration software pipeline, described in *The CalFUSE Pipeline Reference Guide*² (Dixon et al. 2003), but with the following modification: The first half of the pipeline, which corrects for time-dependent effects (such as spacecraft jitter) was run separately on each exposure. The resulting position-corrected photon-event lists were combined, using the program TTAG_COMBINE, into a single data file. The second half of the pipeline, which performs background subtraction and spectral extraction (among other tasks), was run on the combined data file. By thus using the entire data set to scale the background model, we optimize its fidelity, an important consideration for faint continuum sources.

The *FUSE* flux calibration, based on theoretical models of white-dwarf stellar atmospheres, is believed accurate to about 10% (Sahnow et al. 2000). Error bars are assigned to the data assuming Gaussian statistics. To increase their signal-to-noise ratio, we bin the spectra by four detector pixels, about half of a resolution element. The FUV spectrum of 2MASX J21362313-6224008 (Fig. 2) shows a power-law continuum with a broad O VI emission feature at the redshift of the AGN. Selected spectral regions showing redshifted absorption features are presented in Fig. 3.

3. SPECTRAL ANALYSIS

Because the four channels are essentially independent spectrographs, they have different line-spread functions, and their data cannot be safely combined into a single spectrum. Instead, we use only the spectrum from the channel with the highest sensitivity at the wavelength of interest. We identify statistically-significant absorption features with a simple routine that bins each spectrum to the instrument resolution and flags regions whose flux lies more than three standard deviations below the local median. Most of these features are due to the interstellar medium (ISM) of our Galaxy, but a handful share the redshift of the AGN: Ly γ λ 973, C III λ 977, Ly β λ 1026, O VI $\lambda\lambda$ 1032, 1038, and C II λ 1036 (Fig. 3).

Absorption-line profiles are modeled with the interstellar line-fitting package written by M. Hurwitz and V. Saba. Wavelengths, oscillator strengths, and other atomic data are taken from Morton (1991). Given a column density and Doppler broadening parameter, the program computes a Voigt profile for each absorption feature and produces a high-resolution (0.001 Å) spectrum of τ versus wavelength. The model spectra are convolved with a Gaussian of FWHM = 0.08 Å, roughly the spectral resolution of our data, and rebinned to 0.01 Å.

³The Image Reduction and Analysis Facility (IRAF) is distributed by the National Optical Astronomy Observatories, which is operated by the Association of Universities for Research in Astronomy, Inc., (AURA) under cooperative agreement with the National Science Foundation.

Model spectra are fit to the data using the nonlinear curve-fitting program SPECFIT (Kriss 1994), which runs in the IRAF³ environment. SPECFIT performs a χ^2 minimization of the model parameters. Error bars for a particular parameter are derived by fixing that parameter at the best-fit value, then raising it, allowing the other model parameters to vary freely, until χ^2 is increased by 1, which corresponds to a 1σ deviation for a single interesting parameter (Avni 1976).

We begin with the segment of the LiF 1A spectrum shown in the top panel of Fig. 3, which includes the redshifted Ly γ λ 973 and C III λ 977 lines and Galactic O VI $\lambda\lambda$ 1032, 1038 absorption at two velocities. Comparison with data taken during orbital night (not shown) indicates that Ly γ is well separated from the geocoronal O I λ 1028 emission line. The redder O VI λ 1038 line is contaminated by $J=1$ H₂ absorption. Assuming a linear continuum over the wavelength region 1028.4–1038.6 Å, we model all nine species/velocity components labeled in Fig. 3. We constrain the depth of the H₂ line by fitting two other $J=1$ H₂ lines in the 1049–1052 Å range simultaneously. Derived parameters for the Galactic O VI lines are presented in Table 1 and those for the redshifted features in Table 2.

To model the redshifted Ly β λ 1026 feature, we use data from the SiC 1A channel (middle panel of Fig. 3), as the more sensitive LiF channels do not include this wavelength range. The Ly β line falls between a pair of geocoronal emission features due to N II* $\lambda\lambda$ 1084.6, 1087.5. The pair of N II λ 1084 absorption features is interstellar. A comparison with the night-only spectrum (not shown) indicates that N II* λ 1084.6 does not contribute significantly to this spectrum and that the narrow peak on the blue shoulder of the N II* λ 1087.5 line is probably not geocoronal, but intrinsic to the target spectrum. Diffuse emission filling the LWRS aperture yields a line profile that is well approximated by a top-hat function with a width of $\sim 106 \text{ km s}^{-1}$. The N II* λ 1087.5 line is even broader, which also suggests that a second emission component is present. We model the region between 1081 and 1088 Å with a linear continuum, a pair of interstellar N II features, and a redshifted Ly β line. We model the emission feature with a 106 km s^{-1} top hat and a narrow Gaussian. Derived parameters for the redshifted Ly β line are presented in Table 2.

Finally, we turn to the redshifted O VI $\lambda\lambda$ 1032, 1038 and C II λ 1036 features in the LiF 2A spectrum (bottom panel of Fig. 3). These features fall on the broad peak of the redshifted O VI emission feature, which is well fit by a linear continuum. The apparent absorption features at 1095.2 and 1098.5 Å are detector artifacts. The pair of Fe II λ 1097 lines represents absorption from two velocity components in the ISM of our Galaxy. This velocity structure is repeated in Fe II lines at longer wavelengths. As with the Galactic O VI lines, we fit both components of the O VI doublet simultaneously and quote a single set of derived parameters in Table 2.

If the absorbing cloud(s) cover only part of the emitting region, then our derived column densities are lower limits. Alternatively, if the absorption features that we have fit with a single velocity component are due to multiple unresolved clouds, then our derived column densities are upper limits. To investigate the importance of these effects, we calculate the covering fraction of the O VI-absorbing gas as a function of velocity $C_f(v)$ by comparing the depths of the two components with their expected 2:1 ratio. Following the recipe given by Hamann (1997), we find that C_f for the O VI-absorbing gas ranges from 0.5 to 1.0 across the line. Though the error bars are large, this range of values suggests that multiple velocity components are partially resolved in our data. A second velocity component fit to the O VI doublet is, however, significant at only the 2σ level. We therefore assume a single velocity component with a covering fraction $0.5 \leq C_f \leq 1.0$ in the analysis that follows.

Misalignments among the four *FUSE* channels can lead to offsets in the wavelength scales of their spectra. To correct for such offsets, we measure the positions of ISM features in each spectrum and adjust their velocities to a common scale. Our standard is the LiF 1A spectrum, as data from this channel are used to guide the spacecraft. Specifically, we measure the Ar I $\lambda\lambda 1048, 1067$ lines in the LiF 1A spectrum, Ar I $\lambda 1048$ in SiC 1A, and Fe II $\lambda 1097$ in LiF 2A. Absolute velocities remain uncertain, however, because an offset in the position of the target relative to the center of the LWRS aperture can lead to a zero-point uncertainty in the *FUSE* wavelength scale of up to ± 0.15 Å. This uncertainty is not included in our quoted error bars.

Though a detailed analysis of intrinsic emission in the spectrum of 2MASX J21362313-6224008 is beyond the scope of this paper, we can provide a brief description of the salient features. At long wavelengths, the continuum follows a power law of the form $f \propto \lambda^{-\alpha}$, where $\alpha = 5.3 \pm 0.2$. There is a spectral break at the wavelength of Galactic Lyman β , and the spectrum continues flat to the Lyman limit. The O VI feature that dominates Fig. 2 is well fit by a pair of broad O VI emission lines (FWHM = 6280 ± 160 km s⁻¹) and a pair of narrow O VI emission lines (FWHM = 1060 ± 150 km s⁻¹), where all lines are fit with Gaussian profiles. Our target is similar to NGC 3783 in that broad emission from Ly β and higher-order Lyman lines is negligible (Gabel et al. 2003).

4. DISCUSSION

Derived parameters for the Galactic O VI lines are presented in Table 1, and those for the redshifted features in Table 2. The Lyman β and γ lines yield consistent values for the redshifted H I column density and Doppler parameter b . We adopt a value of $N(\text{H I}) = 10^{15}$ cm⁻² in our analysis.

4.1. Photoionization modeling

The redshifted H I, C II, C III, and O VI lines indicate the presence of ionized gas in the neighborhood of the AGN (e.g., Crenshaw et al. 1999) moving away from the central source with a speed of $\sim 310 \text{ km s}^{-1}$ (Table 2). Photoionization models can be used to constrain the parameters of the absorbing gas. We use Cloudy v.94 (Ferland 1996) to calculate the fractional abundance f_{ion} of an element in a given ionization state, assuming the illuminating continuum described by the Cloudy “table agn” model, an absorbing gas with solar abundances and total hydrogen density $n(\text{H}) = 10^5 \text{ cm}^{-3}$ and a grid of values for the total hydrogen column density N_H ⁴ and ionization parameter U . The measured SED of 2MASX J21362313-6224008 (Fig. 1) is consistent with the “table agn” model employed in the calculation; other studies (e.g., Romano et al. 2002) indicate that the use of other SEDs for the illuminating spectrum results in only minor changes to the derived values of N_H and U . We compare the column densities N_{ion} presented in Table 2 with the predictions of the photoionization model to constrain U and N_H in the absorbing gas.

In Section 3, the covering fraction of the absorbing gas in 2MASX J21362313-6224008 was found to be $0.5 \leq C_f \leq 1.0$, consistent with most other intrinsic UV absorbers in AGN (Crenshaw et al. 1999). Following Arav et al. (2001) and Romano et al. (2002), we plot curves of constant N_{ion} in the $\log(U)$ – $\log(N_H)$ plane in Fig. 4. If the absorbing gas covers only part of the emitting region, then N_{ion} is a lower limit and the allowed region of parameter space lies *above* all the curves in Fig. 4 (see Arav et al. 2001 for details). The total hydrogen column density of warm absorbers in Seyfert galaxies is usually lower than 10^{21} cm^{-2} (Kriss et al. 2000, 2003; Romano et al. 2002; Blustin et al. 2003). Given the constraints of Fig. 4, we tentatively place the UV absorber at $\log(U) = -2$, $\log(N_H) = 20$, keeping in mind that substantially higher column densities are not excluded by our data. Observations of other UV, optical, or X-ray lines are required to further constrain the state of the absorber in this AGN.

If the absorption is due to multiple velocity components, the assumption of a single, uniform cloud breaks down, and this model is not applicable.

⁴The hydrogen density $n(\text{H})$ and column density N_H include atomic and molecular hydrogen in all ionization stages, as defined in the Cloudy v.94 manual (Ferland 1996). In the present model, hydrogen is mostly in atomic form.

4.2. Physical condition of the warm absorber

The ionization parameter is defined as $U = Q(H)/4\pi r_0^2 n(H)c$, where $Q(H)$ is the number of ionizing photons ($E \geq 1$ Ry), $n(H)$ is the total hydrogen number density, c is the speed of light, and r_0 is the distance of the illuminated face of the cloud from the central source. We use the measured 2-10 keV luminosity (3×10^{44} erg s $^{-1}$) in conjunction with the assumed “table agn” SED to derive a flux of $Q(H) = 10^{56}$ s $^{-1}$ ionizing photons for 2MASX J21362313-6224008.

Knowing U , N_H , and the density $n(H)$, one can derive the distance, size, and mass of the absorbing cloud. Our data provide no constraints on the density of the absorber — variability studies or other information such as imaging data are necessary to measure $n(H)$ (e.g., Hamann et al. 1997; Crenshaw et al. 2002) — so we will continue to use the value $n(H) = 10^5$ cm $^{-3}$ assumed by the “table agn” model. Adopting the “best-guess” values of $\log(U) = -2$, $\log(N_H) = 20$ derived above, we find that the illuminated face of the absorber lies $r_0 = 160 U_{-2}^{-1/2} n(H)_5^{-1/2}$ pc from the central source. The size of the absorbing cloud is simply given by $L = N_H/n(H) = 10 N_{H,20} n(H)_5^{-1}$ pc. Since $L \ll r_0$ for a wide range of hydrogen densities $n(H)$, the volume of the warm gas can be approximated as $V \sim 4\pi r_0^2 L \times C_f$, and the mass of the warm absorber is $M \sim 2.1 \times 10^7 U_{-2}^{-1} n(H)_5^{-1} N_{H,20} C_f M_\odot$.

4.3. An intergalactic origin for the absorption lines?

The line of sight to 2MASX J21362313-6224008 intersects several clusters of galaxies, two of which have measured redshifts: A3782 at $z = 0.0557$ and APMCC684 at $z = 0.056$. The difference in redshift between the measured absorption lines ($z \sim 0.0578$) and the two clusters is so small that an alternative interpretation of the absorption lines can be entertained, viz., the source shines through the foreground cluster(s), which cause the redshifted absorption lines.

The center of A3782 lies ~ 26 arcmin from 2MASX J21362313-6224008, which corresponds to approximately 1.8 Mpc (for a Hubble constant of $H_0 = 70$ km s $^{-1}$ Mpc $^{-1}$). The center of APMCC684 is ~ 17.5 arcmin distant, which corresponds to 1.2 Mpc. Clusters of galaxies are known to host hot intergalactic gas ($T \geq 10^7$ K) – too hot to produce the observed absorption lines – and oftentimes a lower temperature phase ($T \sim 10^5 - 10^6$ K; Lieu et al. 1996a,b; Bonamente et al. 2002, 2003) that could contain substantial amounts of O VI, C II, C III, and neutral atomic hydrogen. This warm intergalactic gas has been observed in emission in several clusters (i.e., the “soft excess” phenomenon; Bonamente et al. 2002; Kaastra 2003; Nevalainen 2003), notably in the Coma cluster, where it extends some

2.6 Mpc from the cluster center (Bonamente et al. 2003). Detection of O VI absorption associated with the Local Group of galaxies has been recently reported by Nicastro (2003), and detection of an O VI absorption system associated with another galaxy group was reported by Tripp et al. (2000). Here we investigate the association of the detected absorption systems with the two galaxy clusters A3782 and APMCC684.

We use the soft excess measurements of Bonamente et al. (2003) for the Coma cluster to estimate the amount of low-ionization gas in clusters of galaxies. Several other clusters contain warm gas in amounts comparable (within a factor of a few) to those of the Coma cluster. The warm gas is generally more diffuse than the hot gas (Bonamente et al. 2002), and it could reside either inside the cluster (i.e., *mixed* with the hot gas) or in filamentary structures outside the cluster, as is often seen in hydrodynamical simulations (e.g., Cen & Ostriker 1999). If the warm gas is bound to the cluster, Bonamente et al. (2003) show that it must have a density of $1.5 \times 10^{-3} - 6 \times 10^{-5} \text{ cm}^{-3}$ throughout the cluster. Assuming a cluster radius of ~ 3 Mpc, in agreement with current X-ray measurements, this density implies H I column densities of $\sim 10^{20} - 10^{22} \text{ cm}^{-2}$. The metal abundance of the warm gas is ~ 0.1 solar (Bonamente et al. 2003); this implies total carbon column densities of $N_C \sim 5 \times 10^{15} - 5 \times 10^{17} \text{ cm}^{-2}$ and oxygen column densities of $N_O \sim 10^{16} - 10^{18} \text{ cm}^{-2}$. Figure 5 shows the ionization fractions of the ions of concern as a function of temperature, assuming ionization equilibrium (Mazzotta et al. 1998). Column densities of H I, C II, C III, and O VI predicted by this scenario are therefore consistent, for a wide range of temperatures, with those detected toward 2MASX J21362313-6224008 (Table 2). The warm gas may alternatively reside in filamentary structures with densities of $\sim 10^{-4} - 10^{-5} \text{ cm}^{-3}$ (Davé et al. 2001). In this case, Bonamente et al. (2003) show that the filaments will extend for ~ 10 Mpc outside the cluster, yielding similar ion column densities. In addition, the Doppler parameters b of a warm gas at $T \sim 10^4 - 10^6$ K are fully consistent with the values derived in Table 2 (Spitzer 1978), and similar to those of Tripp et al. (2000).

We conclude that the current data for 2MASX J21362313-6224008 are consistent with the redshifted absorption lines of Table 2 originating from warm gas associated with an intervening galaxy cluster.

5. CONCLUSIONS

We detect Galactic O VI absorption in the direction of 2MASX J21362313-6224008 and H I Lyman β and γ , C II, C III, and O VI absorption at a redshift of $z \sim 0.0578$. The redshifted absorption lines are consistent with a circumnuclear absorber outflowing with a relative velocity of -310 km s^{-1} . We derive constraints on its physical parameters through

photoionization modeling. Alternatively, we suggest that the redshifted absorption may originate in or around a cluster of galaxies located along the line of sight.

This research has made use of NASA’s Astrophysics Data System Bibliographic Services and the NASA/IPAC Extragalactic Database (NED), which is operated by the Jet Propulsion Laboratory, California Institute of Technology, under contract with the National Aeronautics and Space Administration. The authors thank Pat Romano for insightful discussions and for sharing the Cloudy commands for the photoionization calculations. This work is supported by a *FUSE* Cycle 4 Guest Investigator grant from NASA.

REFERENCES

- Avni, Y. 1976, *ApJ*, 210, 642
- Arav, N., et al. 2001, *ApJ*, 561, 118
- Blustin, A. J. et al. 2003, *A&A*, 403, 481
- Bonamente, M., Lieu, R., Joy, M. K., & Nevalainen, J. 2002, *ApJ*, 576, 688
- Bonamente, M., Joy, M. K., & Lieu, R. 2003, *ApJ*, 585, 722
- Cen, R., & Ostriker, J. P. 1999, *ApJ*, 514, 1
- Crenshaw, D. M., Kraemer, S. B., Boggess, A., Maran, S. P., Mushotzky, R. F., & Wu, C. 1999, *ApJ*, 516, 750
- Crenshaw, D. M. et al. 2002, *ApJ*, 566, 187
- Davé, R. et al. 2001, *ApJ*, 552, 163
- Dixon, W. V., Kruk, J. W., & Murphy, E. M. 2003, *The CalFUSE Pipeline Reference Guide*
- Ferland, G. J. 1996, *Hazy, a Brief Introduction to Cloudy*, Univ. of Kentucky Dept. of Physics and Astronomy Internal Report
- Gabel, J. R. et al. 2003, *ApJ*, 583, 178
- George, I. M., Turner, T. J., Yaqoob, T., Netzer, H., Laor, A., Mushotzky, R. F., Nandra, K., & Takahashi, T. 2000, *ApJ*, 531, 52
- Hamann, F., Barlow, T. A., Junkkarinen, V., & Burbidge, E. M. 1997a, *ApJ*, 478, 80
- Hamann, F., Barlow, T. A. and Junkkarinen, V. 1997b, *ApJ*, 478, 87
- Hewitt, A., & Burbidge, G. 1991, *ApJS*, 75, 297
- Kaastra, J. S., Lieu, R., Tamura, T., Paerels, F. B. S. and den Herder, J. W. 2003, *A&A*, 397, 445
- Kriss, G. A. 1994, in *ASP Conf. Ser. 61, Astronomical Data Analysis Software and Systems III*, ed. D. R. Crabtree, R. J. Hanisch, & J. Barnes (San Francisco: ASP), 437
- Kriss, G. A., et al. 2000, *ApJ*, 538, L17

- Kriss, G. A., Blustin, A., Branduardi-Raymont, G., Green, R. F., Hutchings, J., & Kaiser, M. E. 2003, *A&A*, 403, 473
- Lieu, R., Mittaz, J. P. D., Bowyer, S., Breen, J. O., Lockman, F. J., Murphy, E. M., & Hwang, C.-Y. 1996, *Science*, 274, 1335
- Lieu, R., Mittaz, J. P. D., Bowyer, S., Lockman, F. J., Hwang, C., & Schmitt, J. H. M. M. 1996, *ApJ*, 458, L5
- Mazzotta, P., Mazzitelli, G., Colafrancesco, S., & Vittorio, N. 1998, *A&AS*, 133, 403
- Mihalic, D., & Binney, J. 1981, *Galactic Astronomy: Structure and Kinematics*, 2nd ed. (San Francisco: Freeman)
- Moos, H. W., et al. 2000, *ApJ*, 538, L1
- Marshall, H.L., Fruscione, A., & Carone, T. E. 1995, *ApJ*, 439, 90
- Morton, D. C. 1991, *ApJS*, 77, 119
- Nevalainen, J., Lieu, R., Bonamente, M. and Lumb, D. 2003, *ApJ*, 584, 716
- Nicastro F. et al. 2003, *Nature*, 421, 719
- Remillard, R. A., Bradt, H. V., Buckley, D. A. H., Roberts, W., Schwartz, D. A., Tuohy, I. R., & Wood, K. 1986, *ApJ*, 301, 742
- Romano, P., Mathur, S., Pogge, R. W., Peterson, B. M., & Kuraszkiewicz, J. 2002, *ApJ*, 578, 64
- Sahnou, D. J., et al. 2000, *ApJ*, 538, L7
- Schwoppe, A., et al. 2000, *Astron. Nach.*, 321, 1
- Spitzer, L. 1978, *Physical Processes in the Interstellar Medium* (New York: John Wiley & Sons), 37
- Tripp, T. M. and Savage, B. D. 2000, *ApJ*, 542, 42
- Voges, W., et al. 1999, *A&A*, 349, 389

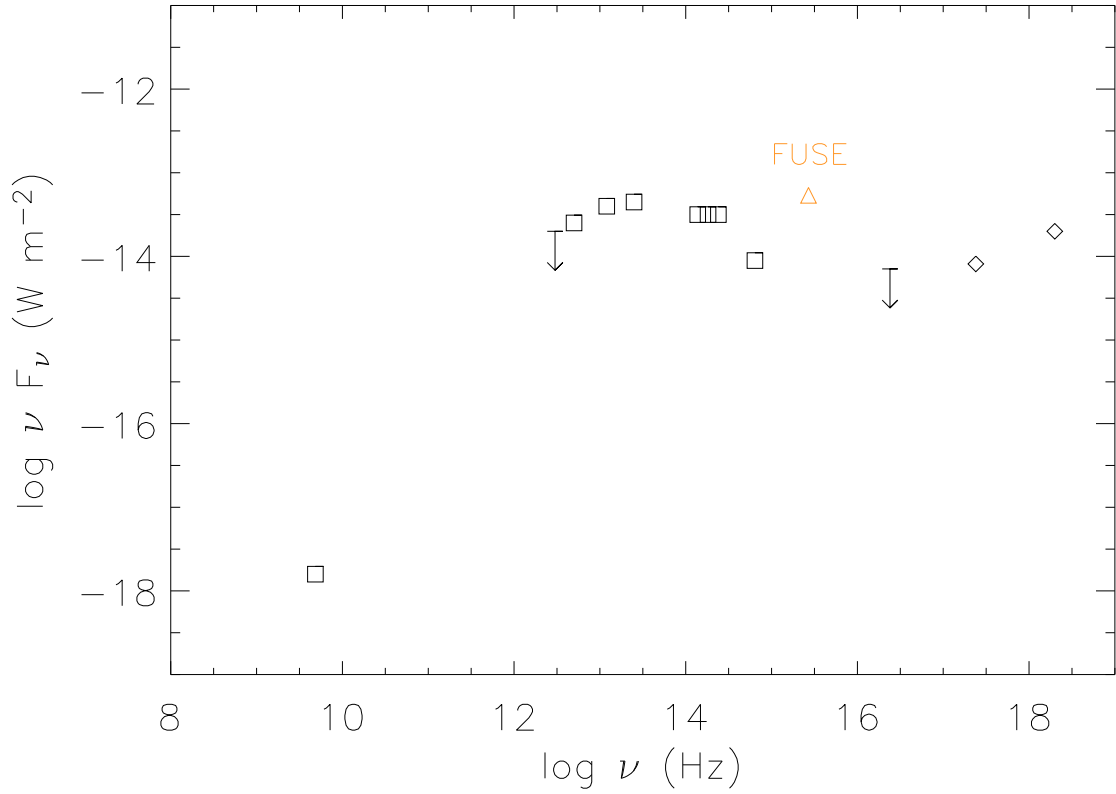


Fig. 1.— Spectral energy distribution of 2MASX J21362313-6224008. To the right of the *FUSE* data point are the *EUVE*, *ROSAT* and *HEAO-1* measurements, respectively. The lower-frequency measurements were derived from the available literature through the NASA/IPAC Extragalactic Database (<http://nedwww.ipac.caltech.edu>).

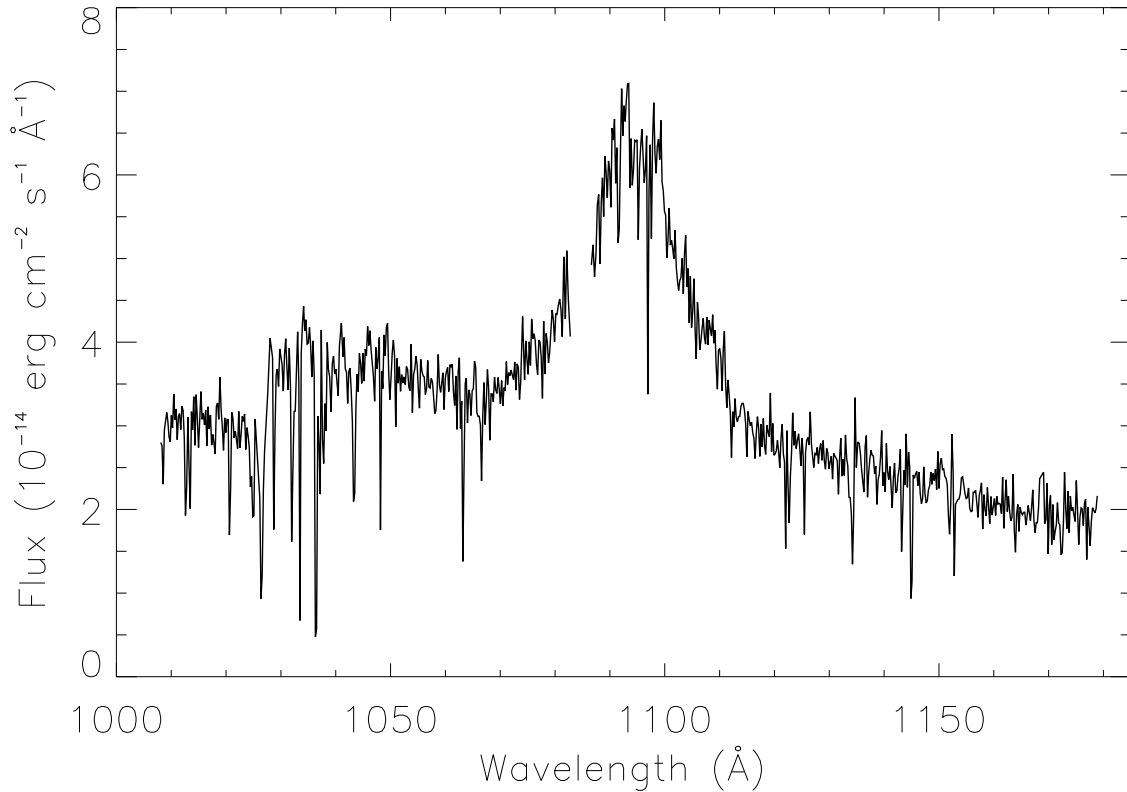


Fig. 2.— *FUSE* spectrum of the Seyfert 1 galaxy 2MASX J21362313-6224008. The data are smoothed by 32 pixels, or about four resolution elements, and geocoronal emission lines (defined as resolved features extending more than three standard deviations above the local median) are excluded. Wavelengths around 1085 Å are not covered by the LiF channels. The spectrum exhibits a power-law continuum with a spectral break at the wavelength of Galactic Lyman β . At shorter wavelengths, the spectrum is flat to the Lyman limit. The broad emission feature is redshifted O VI emission. Most absorption lines are due to the ISM of our Galaxy.

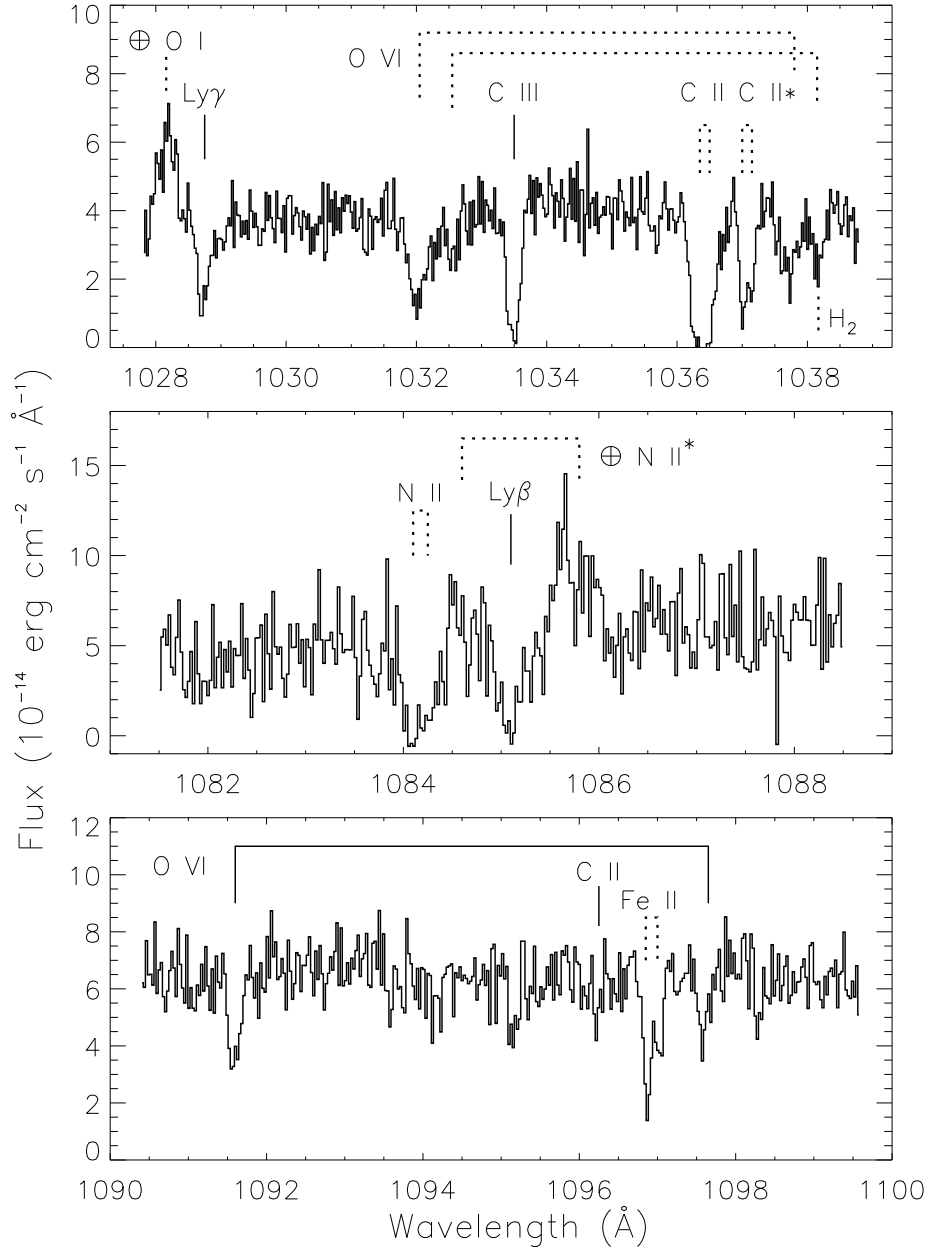


Fig. 3.— Redshifted absorption features in the *FUSE* spectrum of 2MASX J21362313-6224008. Interstellar absorption and geocoronal emission features are marked with dotted lines, redshifted absorption features with solid lines. *Top:* The Ly γ $\lambda 973$ and C III $\lambda 977$ features are blueshifted by 310 km s^{-1} relative to the AGN. The Galactic O VI $\lambda\lambda 1032, 1038$, C II $\lambda 1036$, and C II* $\lambda 1037$ features show two velocity components. *Middle:* Redshifted Ly β absorption falls between the geocoronal N II $\lambda\lambda 1094.6, 1085.7$ emission lines. *Bottom:* Redshifted O VI $\lambda\lambda 1032, 1038$ and C II $\lambda 1036$ with Galactic Fe II $\lambda 1097$ (two velocity components). The apparent absorption features at 1095.2 and 1098.5 \AA are detector artifacts.

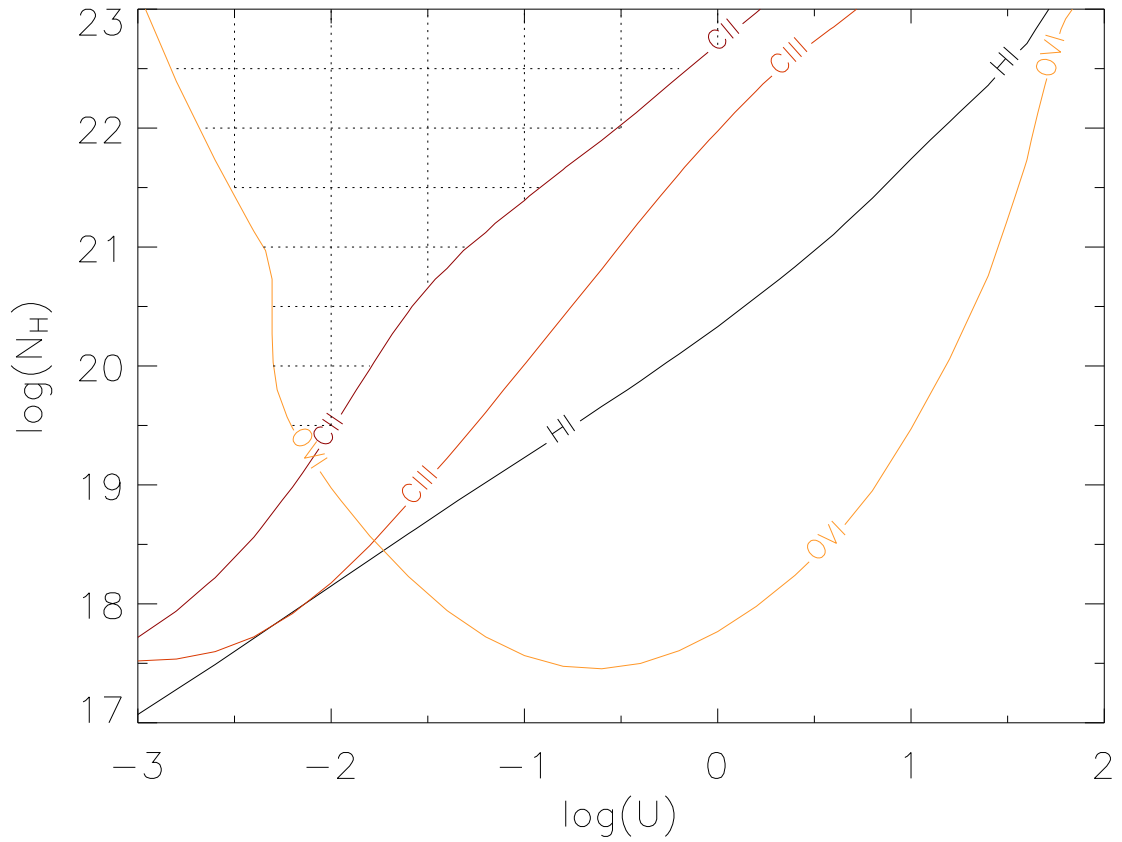


Fig. 4.— Photoionization curves at constant ionic column density. U is the ionization parameter and N_H the total hydrogen column density. The column densities are from Table 2; the H I curve represents a neutral hydrogen column density of 10^{15} cm^{-2} . The cross-hatched area is the region where all constraints are met.

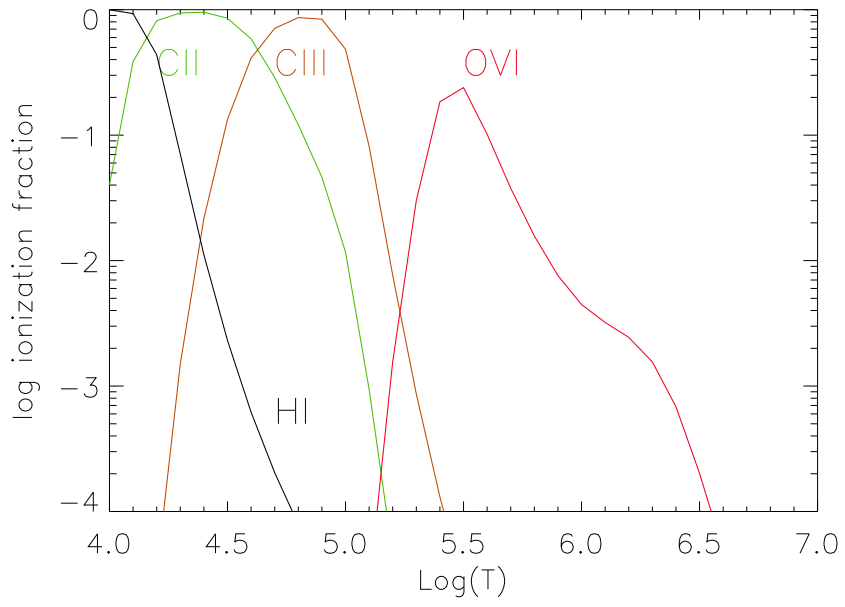


Fig. 5.— Ionization fractions of H I, C II, C III, and O VI for a gas in collisional equilibrium (from Mazzotta et al. 1998).

Table 1. Galactic O VI Absorption Features

Velocity (km s ⁻¹)	Doppler Parameter (km s ⁻¹)	Column Density log N (cm ⁻²)
27 ± 3	53 ± 6	14.44 ± 0.03
175 ± 6	26 ± 15	13.77 ± 0.09

Note. — Velocities are quoted relative to the local standard of rest (LSR; Mihalas & Binney 1981).

Table 2. Redshifted Absorption Features

Feature	Redshift	Velocity (km s ⁻¹)	Doppler Parameter (km s ⁻¹)	Column Density log N (cm ⁻²)
Lyman γ λ 972.5	0.057760(7)	-312 ± 2	27 ± 5	14.97 ± 0.05
C III λ 977.0	0.057783(5)	-305 ± 1	24 ± 3	13.95 ± 0.06
Lyman β λ 1025.7	0.057770(15)	-309 ± 3	26 ± 9	14.89 ± 0.14
O VI $\lambda\lambda$ 1031.9, 1037.6	0.057783(9)	-305 ± 3	20 ± 2	13.95 ± 0.05
C II λ 1036.4	0.057760(87)	-312 ± 3	6 ± 10	13.45 ± 0.16

Note. — In column 2, the digits in parentheses represent the one-standard-deviation uncertainty in the final digits of the redshift. In column 3, velocities are quoted relative to the systemic velocity of 2MASX J21362313-6224008 ($z = 0.0588, cz = 17,630$ km s⁻¹).